Acta Crystallographica Section D
Biological Crystallography
ISSN 1399-0047

Structures of an Eph receptor tyrosine kinase and its potential activation mechanism

Qiang Wei,[a] Jun Liu,[b] Nan Wang,[a] Xiaoying Zhang,[a] Jin Jin,[a] Ian Chin-Sang,[b] Jimin Zheng[a]* and Zongchao Jia[c]*

[a]College of Chemistry, Beijing Normal University, Beijing 100875, People's Republic of China, [b]Department of Biology, Queen's University, Kingston, Ontario K7L 3N6, Canada, and [c]Department of Biomedical and Molecular Sciences, Queen's University, 99 University Avenue, Kingston, Ontario K7L 3N6, Canada

Correspondence e-mail: jimin_z@bnu.edu.cn, jia@queensu.ca

Received 28 June 2014
Accepted 6 October 2014

PDB references: EphA2 kinase, 4pdo; 4p2k; 4trl

Eph receptor tyrosine kinases (RTKs) and their ephrin ligands play a crucial role in both physiological and pathophysiological processes, including tumourigenesis. A previous study of Eph RTKs established a regulatory role for the juxtamembrane segment (JMS) in kinase activation through the phosphorylation of two tyrosines within the JMS. Here, structures of EphA2 representing various activation states are presented. By determining the unphosphorylated inactive and phosphorylated active structures as well as an alternative conformation, conformational changes during kinase activation have been revealed. It is shown that phosphorylation of a tyrosine residue (Tyr772) in the activation loop without direct involvement of the JMS is sufficient to activate the EphA2 kinase. This mechanistic finding is in contrast to the mechanism of other Eph RTKs, such as EphB2, in which phosphorylation of the two JMS tyrosines initiates the dissociation of the JMS and triggers activation-loop phosphorylation for kinase activation. Furthermore, experiments demonstrate that the EphA2 substrate PTEN, a phosphatase that has been implicated in tumour suppression, acts to regulate the phosphorylation states of EphA2, exemplifying a unique reciprocal enzyme–substrate system. Based on these studies, it is therefore suggested that EphA2 may possess an alternate activation mechanism distinct from other Eph RTKs.

1. Introduction

Eph receptor/ephrin signalling mediates diverse developmental processes, such as embryonic patterning, neuronal targeting and vascular development during embryogenesis (Klein, 2004; Lackmann & Boyd, 2008; Mosch *et al.*, 2010). Eph receptor/ephrin signalling is also widely implicated in cancer formation and progression (Dodelet & Pasquale, 2000; Pasquale, 2010). For example, EphA2 is upregulated in a wide variety of cancers, including breast, ovarian, prostate, pancreatic and lung cancers (Ireton & Chen, 2005; Landen *et al.*, 2005; Wykosky & Debinski, 2008).

The Eph receptors comprise the largest family of receptor tyrosine kinases (RTKs) and are divided into two subclasses, namely A and B, based on sequence homology and ligand-binding affinity (Pasquale, 2005). EphA receptors bind primarily to ephrin A ligands, whereas EphB receptors bind mainly to ephrin B ligands. Eph RTKs consist of a glycosylated extracellular region, including an N-terminal ephrin-binding domain, a cysteine-rich region and two fibronectin type III repeats near the single membrane-spanning domain (Murai & Pasquale, 2003). The cytoplasmic region contains a juxtamembrane segment (JMS), a tyrosine kinase domain (KD), a sterile alpha motif (SAM) domain and a C-terminal PDZ binding motif.

Similar to other membrane receptors, ligand binding to the extracellular sites of Eph receptors results in their dimerization and then transphosphorylation through their intracellular kinase domain, leading to receptor activation (Lemmon & Schlessinger, 2010). The enzymatic activation of the intracellular kinase domain occurs through a mechanism involving the phosphorylation of the two conserved tyrosine residues within the JMS (Zisch *et al.*, 2000; Binns *et al.*, 2000). The crystal structure of an unphosphorylated EphB2 comprised of the JMS and the KD reveals the structural basis for this type of receptor activation (Wybenga-Groot *et al.*, 2001). In this structure, the JMS adopts a well ordered, mostly helical structure that interacts intimately with the N-lobe and weakly with the C-lobe to restrict interlobal flexibility. The interaction between the JMS and the C-lobe residue Tyr750 occurs in such a way as to impede the activation segment from adopting an ordered active conformation, a necessary prerequisite for kinase activation. It has been postulated that the interaction between the unphosphorylated JMS and the KD accounts for the arrested autoinhibition states of Eph RTKs, whereas phosphorylation of the JMS tyrosines releases the interaction, which leads to activation.

Surprisingly, a subsequent crystal structure of an unphosphorylated EphA2 containing exclusively the KD appears to suggest a contradictory mechanism (Nowakowski *et al.*, 2002). This structure contains two crystallographically independent molecules, *A* and *B*, in the asymmetric unit. Molecule *B* shows more extensive ordering of the activation segment correlating with a change in the Tyr735 (Tyr750 in EphB2) side-chain rotamer, facilitating a productive path of the activation segment. In contrast, in molecule *A* the Tyr735 rotamer still impedes the activation segment from adopting the active conformation even in the absence of the JMS. Furthermore, the conserved Lys646–Glu663 salt bridge, which coordinates the α and β phosphate groups of ATP, is broken in molecule *A*. Analysis of the JMS-deficient EphA2 structure demonstrates that EphA2 kinase is able to maintain its inactive state even when the inhibitory impact of the unphosphorylated JMS is eliminated. This observation raises the important question of whether the inhibitory role of the JMS is still vital to EphA2 regulation, although there has been no further investigation.

To investigate the activation mechanism of EphA2 further, we crystallized an EphA2 JMS-KD construct both alone and after treatment with a dual-specificity phosphatase, PTEN, which has been implicated in a reciprocal enzyme–substrate system with the EphR homologue VAB-1 in *Caenorhabditis elegans* (Brisbin *et al.*, 2009). We were able to capture three structures corresponding to three different activation states of EphA2: unphosphorylated inactive and phosphorylated active structures, along with an alternative conformation. The structure of unphosphorylated inactive EphA2 represents a new conformation of the JMS that in our structure is remote from the KD C-lobe and does not lock the N- and C-terminal lobes of the KD into an unproductive conformation as in EphB2, indicating that the autoinhibitory function of the JMS is essentially abolished in EphA2. Moreover, for the first time, the highly ordered activation segment, which contains a phosphorylated tyrosine, is captured in the active structure of EphA2. This set of structures mimics steps in the process of kinase activation in EphA2 and reveals that the activation of EphA2 is triggered by phosphorylation of the tyrosine within the activation segment instead of the two tyrosine residues within the JMS. Furthermore, we show that PTEN, an EphA2 substrate, acts to regulate EphA2 kinase activity, demonstrating a reciprocal enzyme–substrate system.

2. Materials and methods

2.1. Protein expression and purification

The coding sequence for the human EphA2 intracellular region (residues 590–876) was cloned into MCS1 of pColA-Duet-1 such that the resultant recombinant clone contains a 6×His tag at the N-terminus. The plasmid was transformed into *Escherichia coli* ArcticExpress (DE3) cells and protein overexpression was induced with 0.2 m*M* isopropyl β-D-1-thiogalactopyranoside (IPTG) at 283 K for 24 h. The protein was purified by nickel-affinity chromatography followed by size-exclusion chromatography (HiLoad 16/60, Superdex 200; GE Healthcare). The purified protein was concentrated to $\sim$6 mg ml^{-1} in 25 m*M* Tris–HCl pH 7.5, 100 m*M* NaCl, 2 m*M* DTT.

The coding sequence for human PTEN containing residues 7–353 was cloned into the pFastBac1 vector such that the resultant recombinant clone contains a 6×His tag at the N-terminus. Recombinant baculovirus was generated using the Bac-to-Bac system (Invitrogen) and Sf21 cells were infected for large-scale protein production. The cells were harvested 48 h post-infection and resuspended in 25 m*M* Tris–HCl pH 7.5, 100 m*M* NaCl supplemented with protease inhibitors and DNase. The protein was purified by nickel-affinity chromatography and stored at 193 K prior to use.

2.2. Crystallization and data collection

Phosphorylated EphA2 was crystallized alone at 293 K by the hanging-drop vapour-diffusion method from 0.1 *M* HEPES pH 7.0, 0.2 *M* Li_2SO_4, 20%(*w*/*v*) PEG 3350. To obtain unphosphorylated EphA2, the purified protein was treated with a small amount of PTEN for $\sim$2 h at 277 K and then concentrated to $\sim$6 mg ml^{-1} before crystallization screens were performed, similarly to the process used with the phosphorylated form. Crystals were obtained from two reservoir conditions: 0.8 *M* sodium/potassium L-(+)-tartrate, 0.1 *M* Tris–HCl pH 8.5, 1%(*w*/*v*) PEG MME 5000 for the unphosphorylated, inactive EphA2 and 0.2 *M* ammonium citrate tribasic pH 7.0, 20%(*w*/*v*) PEG 3350 for the alternative structure of EphA2. Data sets were collected on the NW12A and BL5A beamlines at the Photon Factory, High-Energy Accelerator Research Organization (KEK), Japan. All data sets were processed with *HKL*-2000 (Otwinowski & Minor, 1997).

2.3. Structure determination, refinement and analysis

The structures were determined by molecular replacement using *Phaser* (McCoy *et al.*, 2007). An initial molecular-

replacement model was obtained using PDB entry 1mqb (Nowakowski *et al.*, 2002) after removing all waters and nonbonded ions. Model building and refinement were performed using *Coot* (Emsley & Cowtan, 2004) and *phenix.refine* (Afonine *et al.*, 2012), respectively. The figures were generated using *PyMOL* (Schrödinger). The atomic coordinates and structure factors have been deposited in the Protein Data Bank as entries 4pdo for the inactive structure, 4p2k for the alternative conformation and 4trl for the active EphA2 structure.

2.4. Mutagenesis and Western blot analyses

The cDNA sequence for the JMS and KD of human EphA2 comprised of amino acids 585–876 (corresponding to residues 599–890 of murine EphB2) was cloned into MCS1 of pETDuet-1. Site-directed mutagenesis was used to generate the Tyr588Phe and Tyr594Phe mutations; all mutations were confirmed by DNA sequencing. The constructs were transformed into *E. coli* ArcticExpress (DE3) cells and overexpression was induced with 0.2 m*M* IPTG at 283 K for 24 h. Subsequently, the cells were harvested and lysed in 25 m*M* Tris–HCl pH 7.5, 100 m*M* NaCl, 2 m*M* DTT supplemented with PMSF. The lysates were resolved by 12% SDS–PAGE, transferred onto PVDF membrane and probed using anti-pTyr (Santa Cruz Laboratories) and anti-His antibodies.

2.5. *In vitro* kinase/phosphatase assay

The cDNA sequence of full-length human PTEN was cloned into the pGEX4T1 vector to allow the expression of a GST-fusion protein. GST-PTEN D92A was prepared using the QuikChange site-directed mutagenesis kit (Stratagene). The template for GST-PTEN C124S was the FS60 strain (*daf-2 (e1370) III; daf-18 (mg198) IV; fsEx60*), a *C. elegans* strain overexpressing human PTEN C124S. An expression construct of the human EphA2 intracellular region with an N-terminal MBP tag was constructed by cloning the cDNA sequence of the human EphA2 intracellular region (amino acids 559–976) into the pColADuet-1 vector (Novagen). The MBP sequence was subcloned from the pMalp2x vector (NEB) into the same vector to produce the MBP-EphA2 fusion protein.

MBP-EphA2 and GST-PTEN were co-expressed in the Tuner (DE3) strain of *E. coli*. Soluble fractions were purified on GST-affinity resin (Novagen). Purified samples containing GST-PTEN and co-purified MBP-EphA2 were further run on SDS–PAGE followed by Western blot analysis using the anti-pTyr antibody 4G10 (Millipore/Upstate). Total MBP-EphA2 was detected by anti-MBP conjugated to HRP (NEB). The total GST-PTEN proteins were detected by anti-GST conjugated to HRP (NEB) or by Ponceau staining. The blocking solution and antibodies for Western blotting were supplemented with 5 m*M* sodium orthovanadate as a phosphotyrosine phosphatase inhibitor.

In addition to the co-expression-based kinase/phosphatase assay, MBP-EphA2, GST-PTEN and its two mutants (D92A and C124S) were also individually expressed in the Tuner (DE3) strain of *E. coli* and purified using amylose resin and GST-affinity resins, respectively. 100 ng of MBP-EphA2 kinase and the respective substrates (including GST-PTEN and its D92A and C124S mutants) were mixed with phosphatase buffer (100 m*M* HEPES pH 7.0, 150 m*M* NaCl, 1 m*M* EDTA, 5 m*M* DTT) in each phosphatase reaction at 303 K for 30 min and Na_3VO_4 was used as a pTyr phosphatase inhibitor. Samples were further run on SDS–PAGE followed by Western blot analysis using the anti-pTyr antibody 4G10 (Millipore/Upstate). Total MBP-EphA2 and GST-PTENs were detected by anti-MBP and anti-GST conjugated to HRP, respectively.

To perform an *in vitro* kinase assay, GST-PTEN (wild type) purified from *E. coli* Tuner (DE3) cells was also treated with purified His-EphA2. 100 ng of kinase and substrate were mixed and suspended in kinase buffer (25 m*M* Tris–HCl pH 7.5, 2 m*M* DTT, 0.1 m*M* Na_3VO_4, 10 m*M* $MgCl_2$, 200 µ*M* ATP) for a kinase assay reaction at 303 K for 30 min, while the control group was treated without $MgCl_2$ and ATP in the buffer. Samples were further run on SDS–PAGE followed by Western blot analysis using anti-pTyr. Total His-EphA2 and GST-PTEN were detected by anti-His and anti-GST antibodies, respectively.

3. Results and discussion

3.1. A reciprocal EphA2–PTEN inhibition system

In a previous *C. elegans* study, the EphR homologue VAB-1 and the PTEN homologue DAF-18 were found to be substrates of each other. VAB-1/EphR phosphorylates DAF-18/PTEN to affect its stability (Brisbin *et al.*, 2009). To determine whether the relationship between EphA2 and PTEN is conserved in humans and to gain further insights, we conducted kinase assays followed by Western blot analyses on wild-type PTEN and two PTEN mutants, namely C124S and D92A. It has previously been shown that the C124S mutant abolishes the lipid and protein phosphatase activity of PTEN (Myers *et al.*, 1998; Tamura *et al.*, 1998), whereas the D92A mutant reduces the phosphatase activity but retains the ability to bind substrates (Tamura *et al.*, 1999). As observed in Fig. 1(*a*), wild-type PTEN was the worst substrate and the inactive C124S mutant was the best substrate for EphA2 kinase, whereas the partially inactive D92A mutant exhibited moderate substrate activity. The differing phosphorylation levels of the three PTEN variants revealed that PTEN can indeed be phosphorylated by EphA2 and further indicated that these two proteins may form a reciprocal system. Because PTEN negatively regulates EphA2 and reduces its activity, we observed decreased phosphorylation in PTEN itself (Fig. 1*a*). PTEN mutants with no or reduced activities have no or less inhibitory impact on EphA2, resulting in higher PTEN phosphorylation. It is widely known that the phosphorylation of tyrosine kinases is critical for kinase activation (Hunter, 2009). To test whether PTEN indeed reciprocally dephosphorylates EphA2, we performed a phosphatase assay using a co-expression system. As observed in Fig. 1(*b*), the autophosphorylation levels of MBP-EphA2 were lowest when it was co-expressed with wild-type PTEN, whereas the levels were

much higher when it was co-expressed with C124S and D92A mutant PTEN, respectively. This finding suggests that PTEN can reciprocally dephosphorylate EphA2. In order to further confirm the reciprocal relationship, we next sought to assay *in vitro* phosphorylation and dephosphorylation activities using individually expressed and purified recombinant EphA2 and PTEN. As shown in Fig. 1(*c*), autophosphorylated EphA2 exhibits a strong kinase activity towards PTEN. The EphA2 sample was already autophosphorylated when purified from *E. coli*, while the wild-type PTEN did not show any signal of phosphotyrosine. However, when the wild-type PTEN was treated with EphA2 in the kinase assay buffer, the wild-type PTEN exhibited a high phosphorylation level, revealing the kinase activity of EphA2. Similarly, in the presence of wild-type PTEN the phosphorylation level of EphA2 was markedly reduced (Fig. 1*d*; lanes 1 and 5). EphA2 displayed a much higher phosphorylation level when treated with PTEN mutants with no or reduced phosphatase activities (Fig. 1*d*; lanes 1, 2 and 3). Furthermore, when the phosphatase activity of PTEN was inhibited either by the Cys124-to-Ser124 mutation or by the addition of the inhibitor Na_3VO_4, EphA2 maintained a high phosphorylation level that was comparable with that of EphA2 alone. Although the *in vitro* dephosphorylation results are less pronounced than the co-expression system, other factors may have an impact on the PTEN phosphatase reaction. For example, one possibility would be that PTEN expressed in the cell has a certain level of phosphorylation of the PTEN protein (Song *et al.*, 2012), but that the isolation and purification procedure could have altered it, resulting in different activity levels. Additionally, through structure characterization, we show that PTEN can dephosphorylate EphA2 (see below). Thus, we not only confirm the EphA2 (enzyme)–PTEN (substrate) relationship but also demonstrate the reverse PTEN (enzyme)–EphA2 (substrate) association. Taken together, these results point to the identification of a reciprocal human EphA2–PTEN inhibition

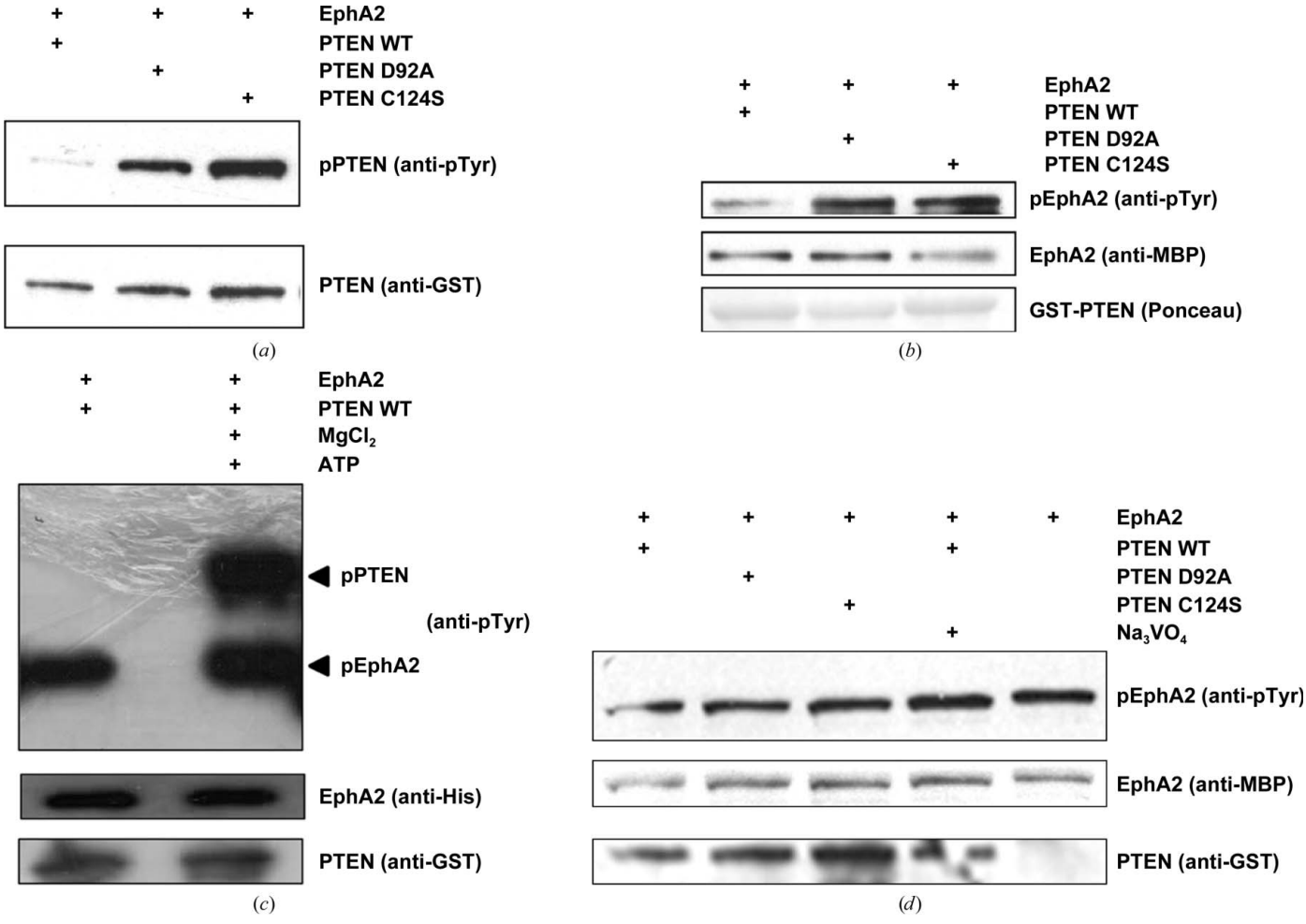

Figure 1
EphA2 and PTEN are substrates of each other. (*a*, *b*) MBP-EphA2 and GST-PTENs were co-expressed in *E. coli* and GST-PTENs were purified on GST resin. The level of phosphorylated PTEN and the autophosphorylation of EphA2 were assayed with anti-phosphotyrosine antibody (anti-pTyr). (*a*) EphA2 phosphorylates phosphatase-dead and phosphatase-deficient PTENs (D92A and C124S) at a much stronger level than wild-type PTEN. (*b*) PTEN dephosphorylates EphA2. MBP-EphA2 physically associates with GST-PTENs and is co-purified on the GST resin. The autophosphorylation level of EphA2 is much lower when co-expressed with wild-type PTEN, suggesting that PTEN can dephosphorylate EphA2. (*c*) Purified EphA2 phosphorylates wild-type PTEN. (*d*) Purified wild-type PTEN dephosphorylates EphA2, while the inhibition of PTEN phosphatase activity results in a higher autophosphorylation level of EphA2.

Table 1
Crystallographic statistics.

Values in parentheses are for the highest resolution shell.

Crystals	Unphosphorylated inactive form	Alternative form	Phosphorylated active form
Data collection			
Space group	$P3_2$	$P2_12_12_1$	$P3_121$
Unit-cell parameters (Å)	$a = b = 92.5$, $c = 75.8$	$a = 54.9$, $b = 74.8$, $c = 76.0$	$a = b = 74.0$, $c = 102.0$
Resolution (Å)	15.0–2.1 (2.14–2.10)	31.2–1.5 (1.53–1.50)	30.0–2.5 (2.49–2.45)
R_{merge}† (%)	8.6 (44.4)	7.9 (17.6)	9.2 (69.7)
Total reflections	196972	358770	69899
Unique reflections	41909 (2082)	50531 (2501)	12263 (588)
Completeness (%)	99.8 (100)	99.4 (100)	99.8 (100)
$\langle I/\sigma(I)\rangle$	19.4 (6.4)	61.6 (14.8)	29.1 (4.2)
Multiplicity	4.7 (5.5)	7.1 (5.9)	5.7 (5.7)
Refinement			
Resolution (Å)	2.1 (2.15–2.10)	1.5 (1.53–1.50)	2.5 (2.70–2.45)
R_{work}/R_{free}‡ (%)	16.0 (15.6)/18.4 (16.6)	17.3 (18.5)/19.0 (18.6)	19.9 (27.1)/25.0 (38.0)
Reflections in work/test set	39764 (2627)/2115 (161)	47973 (2624)/2558 (136)	11642 (2819)/584 (138)
R.m.s.d., bond lengths (Å)	0.007	0.006	0.008
R.m.s.d., bond angles (°)	1.016	1.067	1.190
No. of molecules per asymmetric unit	2	1	1
No. of non-H atoms			
Protein	4184	2070	2146
Water	481	446	43
Average B factors (Å^2)			
Protein	19.7	15.7	38.7
Water	30.1	31.2	34.9
Ramachandran plot, residues in (%)			
Most favoured regions	99.0	98.4	96.1
Additional allowed regions	1	1.6	3.9
Disallowed regions	0	0	0
PDB code	4pdo	4p2k	4trl

† $R_{merge} = \sum_{hkl}\sum_i |I_i(hkl) - \langle I(hkl)\rangle| / \sum_{hkl}\sum_i I_i(hkl)$, where $I_i(hkl)$ is the ith observed intensity and $\langle I(hkl)\rangle$ is the average intensity of all measured observations equivalent to reflection $I(hkl)$. ‡ R_{free} is calculated using 5% of the data, which were set aside for cross-validation.

system in which the reciprocal enzymatic activities mutually inhibit each other.

3.2. Structural characterization of EphA2 in different activation states

An intracellular fragment of human EphA2 consisting of the entire catalytic domain and a partial JMS was expressed in *E. coli*. A phosphorylated active structure of the purified EphA2 protein was first determined at 2.5 Å resolution. Having established the enzyme–substrate reciprocal relationship, we treated EphA2 using PTEN phosphatase in an attempt to capture an unphosphorylated inactive conformation. To this end, we succeeded in obtaining an unphosphorylated inactive EphA2 structure at a resolution of 2.1 Å. Furthermore, we determined an alternative conformation of EphA2 at 1.5 Å resolution. The data-collection and refinement statistics are summarized in Table 1. Similar to other overall structures of RTKs, EphA2 structures feature a bilobed architecture. The N-terminal lobe is composed of the characteristic five-stranded β-sheet (β1–β5) and a single large α-helix (αC). The larger C-terminal lobe is mainly α-helical (αD–αI) but includes a two-stranded antiparallel β-sheet (β7 and β8) (Fig. 2*a*). In addition, the inactive structure of EphA2 presents a highly ordered JMS preceding the kinase domain (Fig. 2*a*). In the inactive structure, interactions of the JMS with another symmetry-related EphA2 molecule are observed, which are likely to be responsible at least in part for the ordering of the JMS as a result of several hydrogen-bonding interactions. The inactive structure is characterized by a broken Lys646–Glu663 salt bridge, whereas both the alternative and the phosphorylated active-state structures maintain this critical salt bridge (see below).

The inactive structure of EphA2 contains no phosphotyrosine residues in the activation segment or in the JMS. The activation segment in EphA2 is completely disordered, just like the unphosphorylated activation segments of other protein kinases (Johnson *et al.*, 1996). Similar to the autoinhibited EphB2 structure, the JMS adopts an identical conformation by folding into two short α-helices (αA′ and αB′) and associates intimately with the αC helix. The αC helix displays a typical bent conformation (Fig. 2*a*), which has previously been shown not to be caused by association with the JMS αB′ helix (residues 598–604; Nowakowski *et al.*, 2002; Wiesner *et al.*, 2006). Interestingly, the N-terminus of the JMS (residues 590–597) is in a very different location to that in autoinhibited Eph kinases such as EphB2 (PDB entry 1jpa; Wybenga-Groot *et al.*, 2001), in which JMS extends along the cleft region between the N- and C-terminal lobes (Fig. 2*b*). The 'strategic' location of JMS in EphB2 restricts interlobal flexibility, thus inhibiting kinase activation. In addition, the interaction between the N-terminus of the JMS and the lobes, especially the position of the unphosphorylated Tyr604, plays an important role in the autoinhibition of EphB2. Tyr604 orients into the hydrophobic pocket between the lobes and causes an alternate conformation of Tyr750. This impedes the activation segment from adopting a productive conformation, which is responsible for the autoinhibition of EphB2 (Wybenga-Groot *et al.*, 2001). In contrast, the N-terminus of the JMS is positioned away from the cleft in EphA2. The absence of the JMS in the cleft would remove inhibition and lead to activation, according to the currently established autoinhibition mechanism of Eph RTKs. However, our structure clearly shows that this is not the case since the JMS-displaced EphA2 structure is still reminiscent of an inactive state. The Lys646–Glu663 salt bridge characteristic of the inactive state is still broken. Other unchanged structural elements include the activation-unfavourable conformation

of Tyr735 (Tyr750 in EphB2) and the disordered activation segment, all of which characterize the inactive state of the kinase (Fig. 2*b*). In a previous brief report, the structure of a JMS-truncated EphA2 (PDB entry 1mqb) was described (Nowakowski *et al.*, 2002). In full agreement with our results, even in the absence of the JMS, one of the two crystallographically independent molecules (molecule *A*) maintains an inactive state similar to that of our dephosphorylated EphA2 (Fig. 2*c*). Thus, we conclude that the role of the JMS in EphA2 is distinct from that in other Eph RTKs.

The 1.5 Å resolution structure of the alternative conformation of EphA2 was obtained by PTEN treatment under different crystallization conditions. In this structure, despite the high resolution, Tyr772 in the activation loop is not visible because part of the activation segment could not be traced owing to a lack of density. No unambiguous phosphotyrosine density was found. We refer to it as an alternative state as it possesses certain structural features that are similar to the active state and other characteristics that are similar to the inactive state. Similar to the active conformation, it maintains the Lys646–Glu663 salt bridge and Tyr735 adopts a non-impeding rotamer conformation that correlates with a more extensive ordering of the activation segment compared with that of the inactive state (Fig. 3*a*). The orientation of Lys646 and Glu663 in the alternative conformation favours the formation of the critical salt bridge, which requires a distance of less than 4 Å (Kumar & Nussinov, 2002). The Tyr735 rotamer conformation is probably caused by a steric clash with Ser761, which is among the residues of the activation segment. All other features are similar to those of the inactive JMS-truncated molecule *B* of EphA2 (Nowakowski *et al.*, 2002), except that the αC in our alternative structure is straighter compared with the fully kinked conformation present in both molecule *B* and the inactive EphA2 state (Fig. 3*b*). The αB′

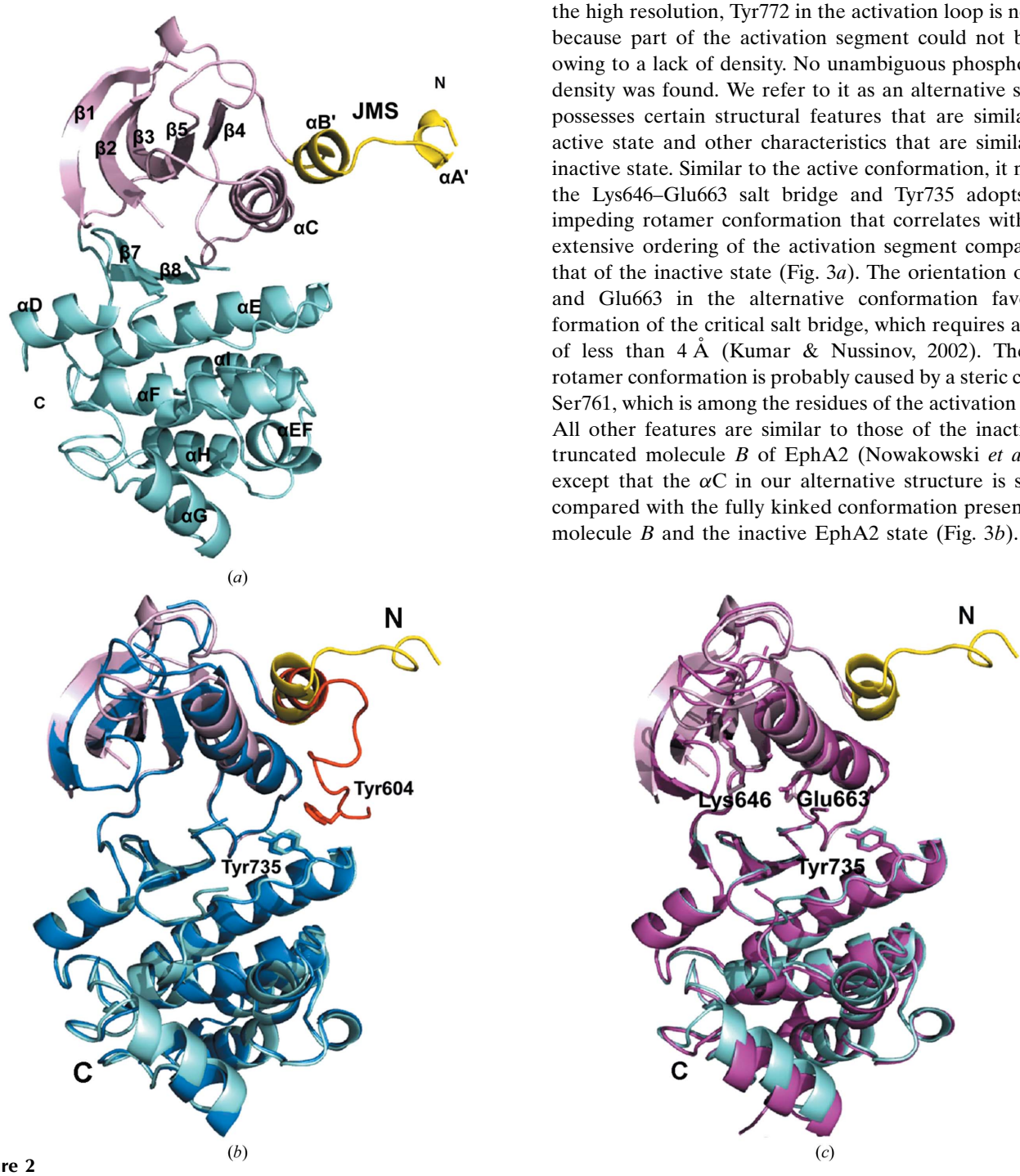

Figure 2
(*a*) Ribbon representation of the structure of inactive EphA2. The JMS, N-terminal lobe and C-terminal lobe are coloured yellow, pink and cyan, respectively. (*b*) Superposition of the structures of inactive EphA2 and autoinhibited EphB2 (PDB entry 1jpa). The backbone of inactive EphA2 is coloured as in (*a*). The JMS of EphB2 is coloured red, whereas the rest of the backbone is blue. All side chains are coloured according to the corresponding backbones. Tyr735 is labelled using the EphA2 numbering scheme, whereas Tyr604 uses the EphB2 numbering scheme. (*c*) Superposition of the structures of inactive EphA2 with molecule *A* of JMS-truncated EphA2 (PDB entry 1mqb). The backbone of inactive EphA2 is coloured as in (*a*) and molecule *A* is shown in magenta. All side chains are coloured according to their respective backbones.

helix of the JMS, which interacts with the αC helix in the inactive structure, changes to a loop, and the N-terminus of JMS is completely disordered. However, instead of staying away from the kinase domain, which was suspected in EphB2, the visible JMS still extends along the KD (Fig. 3*a*).

The 2.5 Å resolution structure of the EphA2 active state was obtained without PTEN treatment. Phosphorylation of Tyr772 was clearly visible in the electron density and the activation segment is highly ordered (Fig. 4*a*). The phosphate makes hydrogen-bonding interactions with residues from the activation segment, such as Arg762, Thr774 and Ser775 (Fig. 4*b*). These interactions help to stabilize the KD in an active conformation. In addition, the Lys646–Glu663 salt bridge is intact, a hallmark of the activated state, along with the activation-favourable rotamer of Tyr735 (Fig. 4*b*). Although the majority of the JMS is disordered, part of αB′ is still visible and maintains limited interaction with αC. Interestingly, even in the active state, the αC helix still displays the bent conformation, which further suggests that a kinked helix αC is a general feature of EphA2.

Overlaying of the structures of the three conformational states revealed that the activation segment, helix αC and the JMS undergo significant conformational changes upon kinase activation (Fig. 4*c*). Given the absence of a negative regulatory role of the JMS in EphA2, the conformational changes observed in the JMS are probably the result of kinase activation rather than the cause. The changes in the αC helix, especially its straighter conformation, observed in the alternative EphA2 structure indicate that αC undergoes conformational exchange upon kinase activation. The same conformational changes of the αC helix were also observed when the activation mechanism of EphB2 was revisited using NMR (Wiesner *et al.*, 2006). Similar to what has been proposed for EphB2, the conserved interaction between αB′ and the αC helix in the inactive state of EphA2 may serve to prevent αC from adopting a catalytically competent conformation. In EphA2, the interaction would be compromised by kinase activation, which is trigged by phosphorylation of the activation segment. Consistent with this notion, previous research has also revealed that mutating Tyr772 to Phe results in reduced kinase activity and hence an impaired ability to phosphorylate the substrates (Miura *et al.*, 2013).

3.3. Function of the juxtamembrane segment in EphA2

In a previous study concerning the functional analysis of phosphorylated tyrosine residues in murine EphA2, an *in vitro*

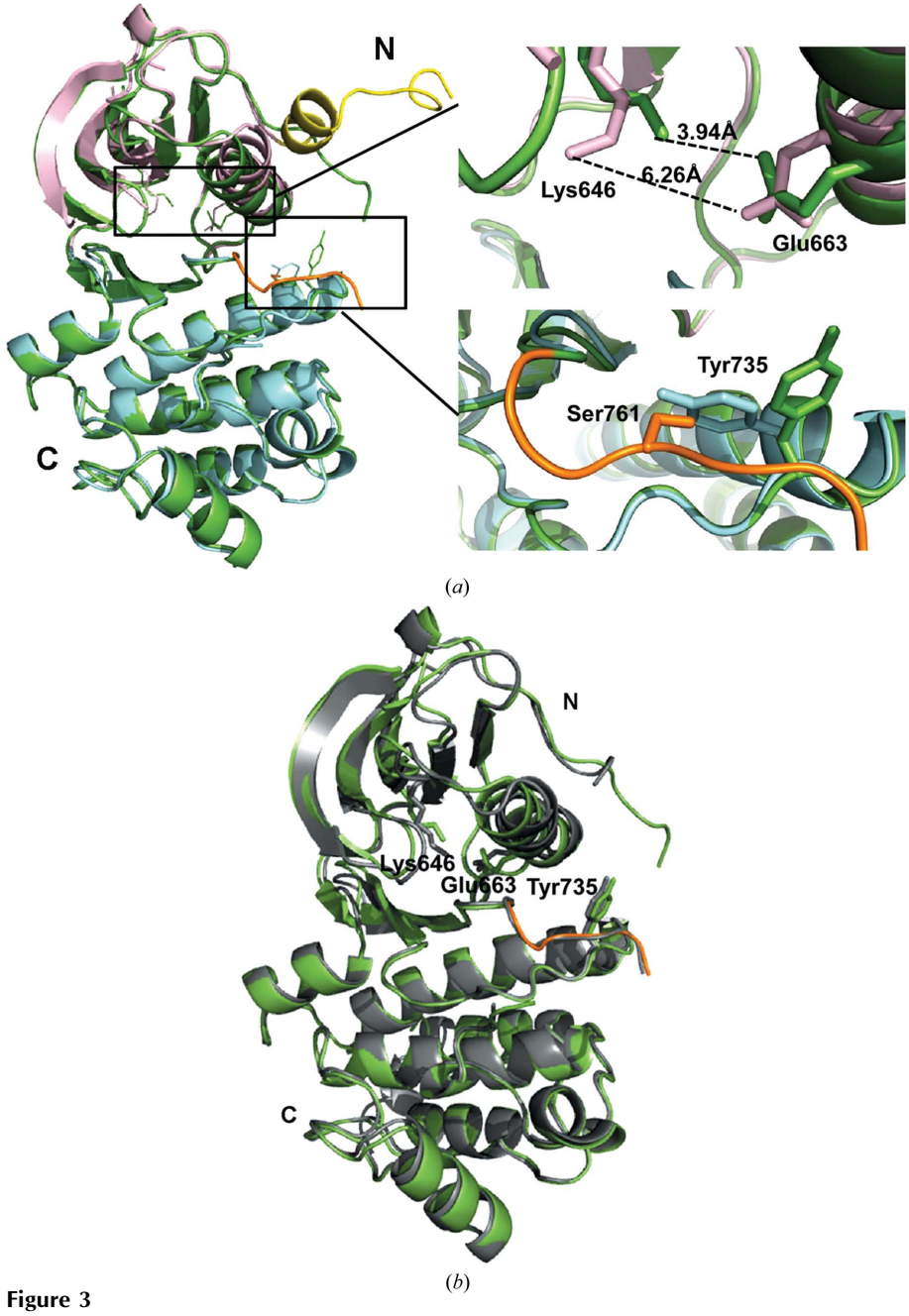

Figure 3
(*a*) Superposition of the alternative and inactive EphA2 structures. The backbone of the alternative EphA2 structure is coloured green, with the activation segment coloured orange. The backbone of inactive EphA2 is coloured as in Fig. 2(*a*). All side chains are coloured according to the corresponding backbones. The measured distances between Lys646 and Glu663 in the different states of EphA2 are labelled. (*b*) Superposition of the structures of the alternative EphA2 structure and molecule *B* of the JMS-truncated EphA2 (PDB entry 1mqb). The backbone and side chains of the alternative EphA2 structure are coloured as in (*a*). The backbone of molecule *B* is depicted in grey and the side chains are coloured according to the corresponding backbone.

kinase assay using different mutants was performed (Fang *et al.*, 2008). The results indicated that the Tyr587Phe (Tyr588 here) and the Tyr593Phe (Tyr594 here) mutants inhibit kinase activity when using a peptide substrate. However, this contradicts the EphA2 autophosphorylation results. Although it is difficult to reconcile the results, we postulate that Tyr587 and Tyr593 may be involved in the ligand-induced receptor-dimerization process when treated with ephrin A1. Thus, they may influence kinase activity indirectly through dimerization instead of directly participating in enzymatic activation. To test our crystallographic findings further, we generated two mutants of the EphA2 JMS-KD fragment in which either Tyr588 or Tyr594 was mutated to phenylalanine. Unlike the impaired kinase activity of the corresponding single mutants of EphB2 (Binns *et al.*, 2000; Zisch *et al.*, 2000), Western blot analyses of the cell lysates with anti-phosphotyrosine antibodies showed that both the Tyr588Phe and Tyr594Phe mutants of EphA2 maintained a high kinase activity (Fig. 5), representing substantial tyrosine phosphorylation of both the receptor itself and cellular proteins compared with wild-type EphA2. Cells transfected by empty vector pETDuet-1, which were used as a negative control, did not show any phosphotyrosine signal, as expected (data not shown). Overall, the mutagenesis results support a different mechanism of kinase activation in EphA2 compared with EphB2, confirming distinct regulatory mechanisms among the Eph receptor family members. This finding further illustrates the unique characteristics of EphA2.

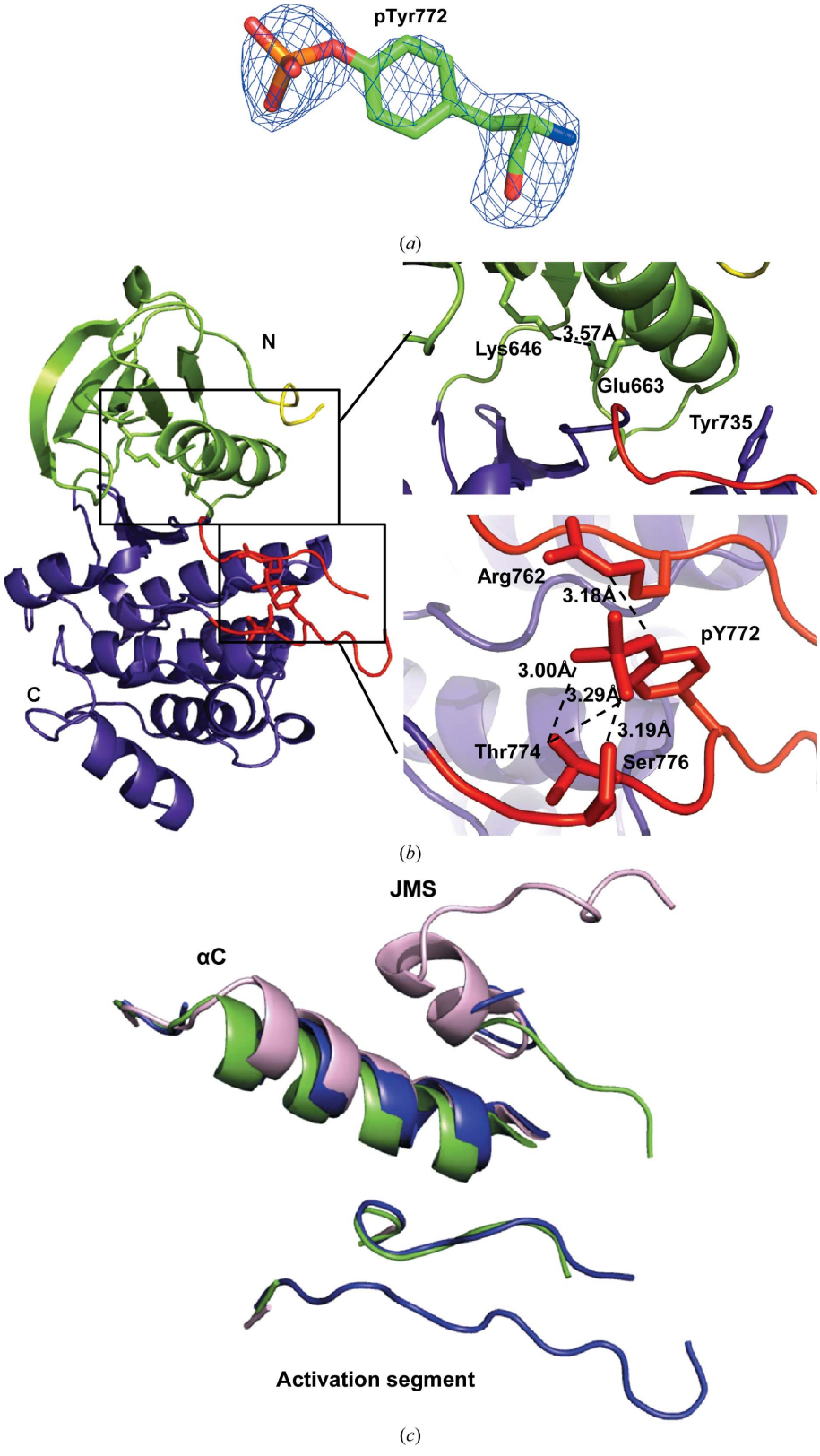

Figure 4
(*a*) The OMIT $F_o - F_c$ electron-density map of phosphorylated Tyr772 at the 3σ level in the EphA2 active structure. (*b*) Ribbon representation of the active structure of EphA2. The partial JMS, N-terminal lobe, C-terminal lobe and extended activation segment are coloured yellow, chartreuse, purple-blue and red, respectively, and the side chains are coloured according to the corresponding backbone. The measured distance between Lys646 and Glu663 in the active state of EphA2 is labelled. Selected hydrogen-bonding interactions involving the activation-loop residues of EphA2 are also shown as black dashed lines and labelled with the corresponding bond distances. (*c*) Superposition of the JMS, αC and activation segment of the three states of EphA2: the inactive, alternative and active states. The structures of the three states are coloured pink, green and purple-blue, respectively.

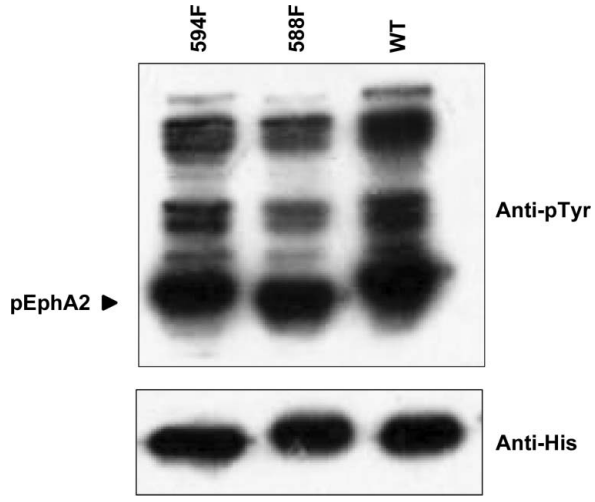

Figure 5
Comparison of the kinase activities of wild-type EphA2 and mutant derivatives. The His-EphA2 proteins were expressed in *E. coli* and the cell lysates were subjected to Western blot analysis with anti-pTyr antibody (top panel) and anti-His antibody (lower panel) as a loading control.

4. Conclusions

We have revealed the unique activation mechanism of EphA2 and have identified a novel reciprocal EphA2–PTEN inhibitory system. Interestingly, the difference between the activation of EphA2 and EphB2 by their ligands has been recognized before: EphA2 can be fully activated by dimeric ephrin A1, whereas EphB2 can only be effectively activated by pre-clustered ephrin B1 (Himanen *et al.*, 2009). In addition to the varying modes of interaction between different Eph receptors and ephrins revealed in the abovementioned study, the different activation mechanisms between EphA2 and EphB2 may also account for the discrepant observations. The requirement for ligand pre-clustering is consistent with the activation mechanism revealed by the autoinhibited structure of EphB2. Receptor dimerization induced by dimeric ephrin-A1, which is sufficient to trigger biological activity in other RTKs, is also sufficient for kinase activation of EphA2, which lacks the inhibitory role of the JMS. Furthermore, the negative regulation afforded by PTEN adds an additional level of inhibition and may compensate for the loss of JMS-mediated inhibition. Our reciprocal inhibition results also imply conserved negative regulation of PTEN by EphA2 between *C. elegans* and human. Interestingly, both the overexpression of EphA2 and the loss of PTEN have been discovered separately to contribute to trastuzumab resistance among breast cancer patients (Zhuang *et al.*, 2010; Nagata *et al.*, 2004).

This work was supported by grants from the National Natural Science Foundation of China (Nos. 21133003 and 21273023) and the Canadian Institutes of Health Research. We would like to thank the staff at the NW12A and BL5A beamlines at the Photon Factory of the High-Energy Accelerator Research Organization, Japan for X-ray data collection.

References

Afonine, P. V., Grosse-Kunstleve, R. W., Echols, N., Headd, J. J., Moriarty, N. W., Mustyakimov, M., Terwilliger, T. C., Urzhumtsev, A., Zwart, P. H. & Adams, P. D. (2012). *Acta Cryst.* D**68**, 352–367.
Binns, K. L., Taylor, P. P., Sicheri, F., Pawson, T. & Holland, S. J. (2000). *Mol. Cell. Biol.* **20**, 4791–4805.
Brisbin, S., Liu, J., Boudreau, J., Peng, J., Evangelista, M. & Chin-Sang, I. (2009). *Dev. Cell*, **17**, 459–469.
Dodelet, V. C. & Pasquale, E. B. (2000). *Oncogene*, **19**, 5614–5619.
Emsley, P. & Cowtan, K. (2004). *Acta Cryst.* D**60**, 2126–2132.
Fang, W. B., Brantley-Sieders, D. M., Hwang, Y., Ham, A.-J. L. & Chen, J. (2008). *J. Biol. Chem.* **283**, 16017–16026.
Himanen, J. P., Goldgur, Y., Miao, H., Myshkin, E., Guo, H., Buck, M., Nguyen, M., Rajashankar, K. R., Wang, B. & Nikolov, D. B. (2009). *EMBO Rep.* **10**, 722–728.
Hunter, T. (2009). *Curr. Opin. Cell Biol.* **21**, 140–146.
Ireton, R. C. & Chen, J. (2005). *Curr. Cancer Drug Targets*, **5**, 149–157.
Johnson, L. N., Noble, M. E. M. & Owen, D. J. (1996). *Cell*, **85**, 149–158.
Klein, R. (2004). *Curr. Opin. Cell Biol.* **16**, 580–589.
Kumar, S. & Nussinov, R. (2002). *Chembiochem*, **3**, 604–617.
Lackmann, M. & Boyd, A. W. (2008). *Sci. Signal.* **1**, re2.
Landen, C. N., Kinch, M. S. & Sood, A. K. (2005). *Expert Opin. Ther. Targets*, **9**, 1179–1187.
Lemmon, M. A. & Schlessinger, J. (2010). *Cell*, **141**, 1117–1134.
McCoy, A. J., Grosse-Kunstleve, R. W., Adams, P. D., Winn, M. D., Storoni, L. C. & Read, R. J. (2007). *J. Appl. Cryst.* **40**, 658–674.
Miura, K., Wakayama, Y., Tanino, M., Orba, Y., Sawa, H., Hatakeyama, M., Tanaka, S., Sabe, H. & Mochizuki, N. (2013). *Oncogene*, **32**, 5292–5301.
Mosch, B., Reissenweber, B., Neuber, C. & Pietzsch, J. (2010). *J. Oncol.* **2010**, 135285.
Murai, K. K. & Pasquale, E. B. (2003). *J. Cell Sci.* **116**, 2823–2832.
Myers, M. P., Pass, I., Batty, I. H., Van der Kaay, J., Stolarov, J. P., Hemmings, B. A., Wigler, M. H., Downes, C. P. & Tonks, N. K. (1998). *Proc. Natl Acad. Sci. USA*, **95**, 13513–13518.
Nagata, Y., Lan, K.-H., Zhou, X., Tan, M., Esteva, F. J., Sahin, A. A., Klos, K. S., Li, P., Monia, B. P., Nguyen, N. T., Hortobagyi, G. N., Hung, M. C. & Yu, D. (2004). *Cancer Cell*, **6**, 117–127.
Nowakowski, J., Cronin, C. N., McRee, D. E., Knuth, M. W., Nelson, C. G., Pavletich, N. P., Rogers, J., Sang, B.-C., Scheibe, D. N., Swanson, R. V. & Thompson, D. A. (2002). *Structure*, **10**, 1659–1667.
Otwinowski, Z. & Minor, W. (1997). *Methods Enzymol.* **276**, 307–326.
Pasquale, E. B. (2005). *Nature Rev. Mol. Cell Biol.* **6**, 462–475.
Pasquale, E. B. (2010). *Nature Rev. Cancer*, **10**, 165–180.
Song, M. S., Salmena, L. & Pandolfi, P. P. (2012). *Nature Rev. Mol. Cell Biol.* **13**, 283–296.
Tamura, M., Gu, J., Danen, E. H., Takino, T., Miyamoto, S. & Yamada, K. M. (1999). *J. Biol. Chem.* **274**, 20693–20703.
Tamura, M., Gu, J., Matsumoto, K., Aota, S., Parsons, R. & Yamada, K. M. (1998). *Science*, **280**, 1614–1617.
Wiesner, S., Wybenga-Groot, L. E., Warner, N., Lin, H., Pawson, T., Forman-Kay, J. D. & Sicheri, F. (2006). *EMBO J.* **25**, 4686–4696.
Wybenga-Groot, L. E., Baskin, B., Ong, S. H., Tong, J., Pawson, T. & Sicheri, F. (2001). *Cell*, **106**, 745–757.
Wykosky, J. & Debinski, W. (2008). *Mol. Cancer Res.* **6**, 1795–1806.
Zhuang, G., Brantley-Sieders, D. M., Vaught, D., Yu, J., Xie, L., Wells, S., Jackson, D., Muraoka-Cook, R., Arteaga, C. & Chen, J. (2010). *Cancer Res.* **70**, 299–308.
Zisch, A. H., Pazzagli, C., Freeman, A. L., Schneller, M., Hadman, M., Smith, J. W., Ruoslahti, E. & Pasquale, E. B. (2000). *Oncogene*, **19**, 177–187.